J. Fluid Mech. (1994), *vol.* 266, *pp.* 147–173

On one-dimensional flow of a conducting gas between electrodes – with application to MHD thrusters

By M. D. COWLEY[1] AND J. H. HORLOCK[2]

[1] Cambridge University Engineering Department, Trumpington Street, Cambridge CB2 1PZ, UK

[2] St John's College, Cambridge CB2 1TP, UK

(Received 8 February 1993 and in revised form 20 October 1993)

Inviscid, adiabatic, one-dimensional flow of a conducting gas in the presence of crossed electric and magnetic fields is investigated for the case where the magnetic field is generated by the current being supplied to the gas. The electrode geometry and the connections to the electrical power supply are such that the magnetic field falls to zero at the downstream end of the MHD duct. The analysis allows for magnetic Reynolds number r_m to be anywhere in the range 0 to ∞. The main part of the investigation is restricted to consideration of ducts with constant spacing between electrodes.

The way in which the density of the gas varies along the duct with the changing magnetic field is analysed generally and the results are then applied to the case where gas is fed to the MHD duct from high pressure in a plenum chamber and where the duct exhausts to a region of negligible pressure. If the flow is choked by the converging entry to the duct and the magnetic Reynolds number is moderate to high, the main electromagnetic effect is for the $\boldsymbol{j} \times \boldsymbol{B}$ forces to accelerate the gas to supersonic speeds. As r_m is reduced, ohmic heating becomes more important, and it may cause the flow to be choked at exit from the duct, giving rise to a reduction in mass flow. For certain ranges of r_m and ratio of initial magnetic pressure to plenum-chamber pressure the flow may choke at a sonic point within the duct itself, while accelerating from subsonic to supersonic through the point.

Some illustrative examples of how properties vary with distance along the duct have been computed and the consequences of the analysis for MHD thrusters are explored. The magnetic forces will augment thrust per unit cross-sectional area, the essential measure of this being the drop in magnetic pressure along the duct, but there is an upper limit on the ratio of magnetic pressure to plenum-chamber pressure for flows to be possible. Flow at low magnetic Reynolds number is favoured if the object is to increase specific thrust by reducing mass flow through the duct.

1. Introduction

One-dimensional flow of an electrically conducing gas through applied electric and magnetic fields has been studied extensively (beginning with Resler & Sears 1958). In such work it was generally assumed that the magnetic field was not changed by the current in the flow (i.e. the magnetic Reynolds number r_m was assumed to be very small).

More recently, Kuriki, Kunii & Shimizu (1983) have described a problem of one-dimensional MHD flow with effective magnetic Reynolds number ranging from low to high. They studied an idealized model for gas acceleration in an MPD arcjet, where the

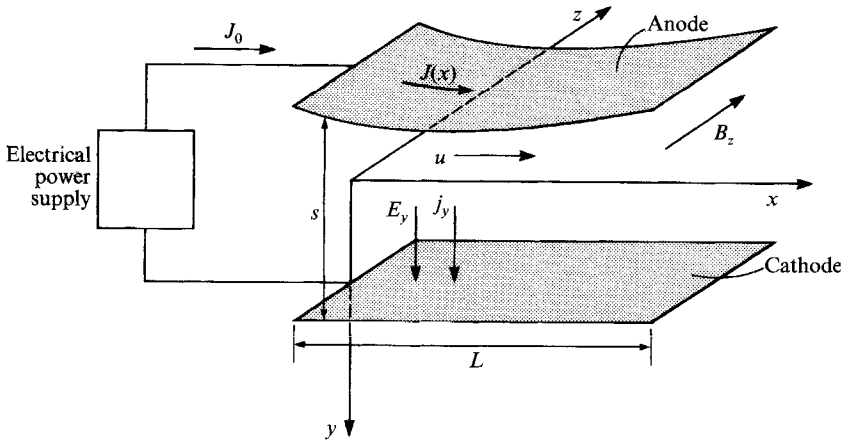

FIGURE 1. Geometry of the annular duct.

magnetic field is self-induced and the geometry is that of figure 1, which shows an annulus of large mean radius. The walls of the annulus form electrodes which are connected to an electrical power supply, so that there may be an electric field E_y and a current flow (of density j_y) across the duct. The magnetic flux of density B_z, associated only with current flow in the gas, is continuous in the tangential z-direction (i.e. round the annulus of large radius) but B_z (and other properties) are taken to be functions of the streamwise coordinate x only.

The assumption of one-dimensionality and the boundary conditions on electric and magnetic fields merit discussion. If the current flow along the upper electrode is $J(x)$ per unit width of electrode, then the current density in the channel j_y is equal to $-\mathrm{d}J/\mathrm{d}x$. The power supply is taken to be connected to the upstream ends of the electrodes and to provide a return path upstream, so that J is zero at the end of the electrodes ($x = L$) and, since there is no current enclosed by the line integral of magnetic flux density round the annulus at $x = L$, that magnetic flux density must be zero. Similarly it follows that the flux density at entry B_0 is directly proportional to the current flow in the electrodes there, $B_0 = \mu J_0$. If the power supply is envisaged as a generator of known current, B_0 will be specified. Note that the current distribution in the gas controls the form of the magnetic field even at very low magnetic Reynolds number, but that the distribution will be affected by the motion at moderate to high values of r_m.

One-dimensionality implies that fringing of electric and magnetic fields is neglected, e.g. at the downstream end of the electrodes, where like Kuriki *et al.* we shall assume the electric field intensity changes from a finite value to zero in a short length. At high values of r_m current boundary layers will tend to form on the walls downstream of where the electrodes end, in order to permit sweeping of the magnetic flux with the flow. The flux distribution in the boundary layers is such that

$$\frac{\partial^2 B_z}{\partial y^2} = O\left(\frac{r_m}{L}\frac{\partial B_z}{\partial x}\right), \tag{1}$$

where the magnetic Reynolds number r_m is based on length of duct L. If the electrode spacing is s, then the length scale of the fringing (from the end of the electrodes to where

the current boundary layers meet) will be $O(r_m s^2/L)$. For small fringing effect, the longitudinal scale of the electrodes L must be large compared with this quantity,

$$L \gg (r_m/L)\, s^2,$$

i.e.
$$L/s \gg r_m^{\frac{1}{2}}$$

is a condition for one-dimensionality. (L/s must anyway be much greater than unity to avoid normal fringing effects at low r_m.)

By assuming the electromagnetic acceleration to be dominant, Kuriki *et al.* were able to obtain magnetic flux and velocity distributions in a one-dimensional duct, essentially for a selected value of their parameter $R_m = \sigma B_0^2 L/G$, where σ is the electrical conductivity and G is mass flow rate per unit area (an average value in cases where cross-sectional area varied). A voltage parameter, $\phi = \mu EG/B_0^3$, was determined so as to give B_z zero at exit from the channel. The relation between ϕ and R_m was found (described by the authors as the voltage–current characteristics of the MPD arcjet).

In the present work, both the geometry and the boundary condition on B_z at $x = L$ ($B_z = 0$) used by Kuriki *et al.* are adopted. Like them, we shall assume that the gas is electrically conducting at entrance to the duct, that the electrical conductivity is unchanged along the duct, and we shall neglect the Hall effect. However, their additional assumption about the dominant magnitude of the electromagnetic acceleration is not made. They dropped the pressure p as a flow parameter, but here it is retained, the flow being assumed to be that of an inviscid, electrically conducting, perfect gas. Most of the analysis refers to ducts with constant spacing between electrodes.

The effect of pressure in one-dimensional MHD flow of the type investigated here was considered by Shercliff (1965), but with a restricted form of the equation of state of the gas. He took the pressure to be directly proportional to the density, implying a constant speed of sound (in the analysis of Kuriki *et al.* speed of sound is effectively zero). A particular feature of Shercliff's analysis was his study of how magnetic flux density B would vary with density ρ along the duct and this proved a powerful tool for elucidating possible flows. We shall therefore adopt a similar approach here, investigating the (B, ρ)-variation, but for a gas with a more conventional equation of state (§§3 and 4). The simplicity of the algebra when p/ρ is taken as constant makes it an attractive assumption and by way of introduction to the main analysis we shall refer further to the consequences of that assumption in §2.

The major difference in the work of this paper from either that of Kuriki *et al.* or that of Shercliff lies in the fact that pressure enters the problem as a function of two thermodynamic variables and an extra conservation equation is needed – the energy equation. This in turn involves an assumption about heat transfer and we take the flow to be adiabatic – a questionable assumption if temperature is high and radiation effects become important. It is within the light of this limitation that we have not thought it worthwhile to use more complex gas property relations than the simple equations for a perfect gas. A further shortcoming is that our model is not able to describe any process by which cold gas fed to the duct might become ionized. However, the model flows are extremely complex and we believe that they are of intrinsic interest as examples of magnetogasdynamic behaviour in spite of the shortcomings.

Nevertheless, it will be found that even with the above assumptions the situation remains highly complex and further limitations have to be imposed on the analysis presented here. First, the full justification of how flow properties vary as the intensity of magnetic field decreases along the duct will not be given, but there is an outline of

the main features of flow behaviour in §3. Readers interested in seeing further details of the justification should apply to the Editorial Office of the *Journal* for a copy of Appendices to this paper which are held there. Secondly we shall concentrate on the application that was the concern of Kuriki *et al.*, namely electromagnetic thrusters. This imposes constraints on the flow states at exit from and inlet to the duct, but still leaves a rich variety of flows. How the occurrence of the different flow patterns depends on overall parameters for the duct is described in §4, but once again, full justification is relegated to the Appendices which are available on request. To illustrate each of the different types of flow pattern, numerical solutions are presented in §5. Some of the consequences of the theory for ideal thrusters are explored in §6.

2. Basic equations

We consider the one-dimensional flow of figure 1, but now drop the subscripts previously used. Local fluid properties are velocity u, pressure p, density ρ, enthalpy h. Local magnetic flux density is B, local current density j, and local electric field intensity $E = V/s$, where V is the voltage applied across the channel, of electrode spacing s.

In differential form, the relevant equations for an inviscid adiabatic flow are:

momentum, $$\frac{\mathrm{d}p}{\mathrm{d}x}+\rho u\frac{\mathrm{d}u}{\mathrm{d}x}=jB; \tag{2}$$

continuity, $$\frac{1}{\rho}\frac{\mathrm{d}\rho}{\mathrm{d}x}+\frac{1}{u}\frac{\mathrm{d}u}{\mathrm{d}x}=-\frac{1}{s}\frac{\mathrm{d}s}{\mathrm{d}x}; \tag{3}$$

energy, $$\rho u\frac{\mathrm{d}h}{\mathrm{d}x}+\rho u^2\frac{\mathrm{d}u}{\mathrm{d}x}=jE; \tag{4}$$

Ampere's law, $$\frac{\mathrm{d}B}{\mathrm{d}x}=-\mu j; \tag{5}$$

and Ohm's law, $$j=\sigma(E-uB). \tag{6}$$

Equation (3) may be integrated directly to give

continuity, $$G=\rho u=m/A, \tag{7}$$

where m is the mass flow rate (constant) and A is the total cross-sectional area of the duct (proportional to electrode spacing s). Substituting for j from (5) in (4), the latter equation may be integrated on noting that ρu and E are both inversely proportional to electrode spacing:

energy, $$H=h+\tfrac{1}{2}u^2=H^0-\frac{EB}{\mu G}, \tag{8}$$

where H^0 is a constant. EB/μ is the Poynting vector and (8) is easily recognized as an expression of the overall balance between the fluxes of enthalpy, kinetic energy and electrical energy.

If the electrode spacing is constant, G of (7) is constant and the momentum equation can then be integrated to give:

momentum, $$F=p+\rho u^2=F^0-\frac{B^2}{2\mu}, \tag{9}$$

where F^0 is constant and we have again substituted for j from (5). Here we may recognize that the equation is an expression of overall balance between pressure, inertia

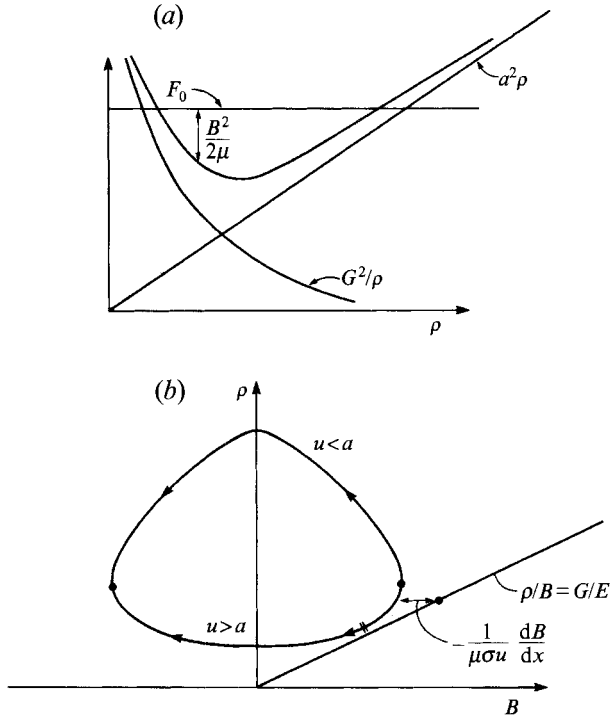

FIGURE 2. (*a*) Relation between terms in the momentum equation for a gas with $p/\rho = \text{const.}$ (*b*) The (B,ρ)-curve for a gas with $p/\rho = \text{const.}$ The arrows indicate the direction of travel along the curve for increasing distance along the MHD duct. ●, Sonic point; \ \, magnetosonic point.

stress and magnetic pressure $B^2/2\mu$. In writing (7) and (8), the notation of ordinary one-dimensional gasdynamics (Shercliff 1958) with the symbols F (impulse function per unit area), G (mass flow per unit area) and H (stagnation enthalpy) has been introduced. In terms of these quantities a Rayleigh process is one with F and G constant, and a Fanno process one with G and H constant, for example.

An elementary type of compressibility is given by pressure being directly proportional to density only (Shercliff 1965). The constant of proportionality, being also equal to $\mathrm{d}p/\mathrm{d}\rho$, is the square of the speed of sound a^2, and (9) becomes

$$\frac{G^2}{\rho}+a^2\rho+\frac{B^2}{2\mu}=F^0. \tag{10}$$

The variation with density of the three terms on the left-hand side of this equation is as shown on figure 2(*a*) and it follows that the path line of the process on a (B,ρ)-plot is a closed loop which is symmetrical about the ρ-axis (see figure 2*b*). The slope of the (B,ρ)-loop is

$$\frac{\mathrm{d}\rho}{\mathrm{d}B}=\frac{B}{\mu(u^2-a^2)}. \tag{11}$$

Three important points follow from this expression, which is still valid if the $p/\rho = \text{const.}$ condition is relaxed to $p = f(\rho)$. First, B is stationary at sonic points ($u = a$ at the extremities of the loop) and ρ is stationary when $B = 0$ (ρ is a maximum or a minimum where the curve crosses the vertical axis). Secondly, a continuous length of curve between the sonic-state extremities must be either supersonic or subsonic. Since $\mathrm{d}\rho/\mathrm{d}B^2$ is positive on the lower part of the loop of figure 2(*b*), that part must be

supersonic, while the upper part is subsonic. Note that there is the possibility of transition by an ordinary gasdynamic shock wave from supersonic to subsonic with $B = \text{const}$. Thirdly, at a point where a straight line from the origin touches the closed loop,

$$\frac{\rho}{B} = \frac{\mathrm{d}\rho}{\mathrm{d}B} = \frac{B}{\mu(u^2 - a^2)},$$

i.e.

$$u^2 = a^2 + B^2/\mu\rho. \tag{12}$$

$B/(\mu\rho)^{\frac{1}{2}}$ is the Alfvén wave speed b and $(a^2+b^2)^{\frac{1}{2}}$ is the speed of magnetoacoustic waves with direction of propagation perpendicular to the magnetic field. Equation (12) therefore implies that the flow is magnetosonic at the tangent point.

The direction of travel on the loop to give an allowable variation of ρ and B with distance follows from consideration of Ohm's law. From (5) and (6) we obtain

$$j = \sigma(E - GB/\rho) = -\frac{1}{\mu}\frac{\mathrm{d}B}{\mathrm{d}x}, \tag{13}$$

so that, for a process in which B is reducing, E must be greater than GB/ρ, i.e. the portion of the (B,ρ)-loop representing that process must lie to the left of the line on which $\rho/B = G/E$ (see figure 2*b*).

To determine the flow in the duct, we need to prescribe entry and exit conditions. Note that it is not enough to specify $B = 0$ for the latter since there are two possible flow states, one supersonic and the other subsonic. As mentioned in §1, we shall concentrate on the application of the analysis to thrusters and we assume first that the duct exhausts into an ambient condition of very low pressure. The exit state cannot then be subsonic. The supersonic state with $B = 0$ can be approached along the lower part of the (B,ρ)-loop provided that any supersonic part involved lies to the left of the $\rho/B = G/E$ line. It is then not possible to find a configuration that allows a continuous variation from subsonic to sonic to supersonic, ending with $B = 0$, since increasing B subsonically would be prohibited. Therefore, the entry state must not be subsonic. Secondly, we limit discussion to the case of gas being supplied to the duct from a plenum chamber via a pure convergence. The inlet state must then not be supersonic and the only possibility is for it to be precisely sonic, i.e. the right-hand sonic point on figure 2(*b*), and from the that state density decreases (i.e. the flow accelerates continuously) to the exit condition. The overall increase in momentum flux of the gas will be somewhat greater than the electromagnetic force applied since the falling density implies that there is also a pressure force in the direction of the flow.

ρ/B takes its lowest value at the magnetosonic point, so that from (13) current density is a minimum there, as will be the rate of change of B with distance. A special case arises when the magnetic Reynolds number tends to infinity and the minimum current density must then tend to zero (i.e. the $\rho/B = G/E$ line must approach tangency to the loop), so that the total current across the duct can remain finite. Near the limit a substantial length of the duct has flow at a condition close to magnetosonic, i.e. $u \to (a^2+b^2)^{\frac{1}{2}}$, with B nearly constant. Such a condition also appears in the solution of Kuriki *et al.* (1983), but in their work $a = 0$, so that the corresponding result is $u \to b$ over most of the duct length.

3. (B,ρ)-variation for a perfect gas

Having established how the magnetic field B varies with the density ρ in the MHD duct when pressure is directly proportional to density, so that the controlling equations are continuity (7) and momentum (9) only, we turn to the problem of (B,ρ)-variation

when pressure is taken to be a function of enthalpy as well as density. Now the energy equation (8) must be added to (7) and (9). However, for brevity, only an outline of the results will be provided here and for further details Appendix A of the Appendices available on request from the Editorial Office of the *Journal* should be consulted.

Some general points about the flow equations can give an impression of what may happen in adiabatic flow when the energy equation is involved. First, if conditions could in some sense be such that the magnetic-pressure term has a strong influence in the momentum equation, while that of the Poynting vector in the energy equation is weak, behaviour will approach that of the well-known Fanno process (G and H constant with F varying). The difference is that the Fanno process is normally taken as a representation of friction opposing the flow, whereas the reducing magnetic pressure corresponds to a force in the flow direction. Strictly, a Fanno process with F increasing is easily shown to be inconsistent with the second law of thermodynamics – entropy would be decreasing under adiabatic conditions – and the implication is that the Poynting vector cannot be wholly discounted. Nevertheless, it is of interest to note that in a Fanno process F is a minimum at a sonic point (see, for example, Shercliff 1958) and the (B,ρ)-curve would be a closed loop, qualitatively like that of a gas with $p/\rho = \text{const.}$ (see figure 3*a*).

Secondly, if the strength of influence of the terms is reversed, conditions will approach those of a Rayleigh process (G and F constant with H varying). For such a process H is a maximum when the flow is sonic (Shercliff 1958) and the (B,ρ)-curve can therefore only exhibit a point of minimum B, and must be as sketched in figure 3(*b*). The point of minimum B may lie on either side of the ρ-axis. Since the shape of the (B,ρ)-curve for a Rayleigh process is significantly different from those considered up to now, it is likely that the combined effects of magnetic pressure and Poynting vector will give rise to some complexity.

The general differential relation for $\mathrm{d}B/\mathrm{d}\rho$ may be easily derived from (2)–(5) if we introduce the thermodynamic parameter $\gamma_h = a^2/(\partial p/\partial\rho)_h$, where $a = (\partial p/\partial\rho)_s^{\frac{1}{2}}$ is the isentropic speed of sound. It may be shown that under general conditions of thermodynamic equilibrium (but the gas not necessarily perfect)

$$\mathrm{d}h = \{\gamma_h/(\gamma_h-1)\}\,\mathrm{d}p/\rho - a^2\{1/(\gamma_h-1)\}\,\mathrm{d}\rho/\rho. \tag{14}$$

Using this result to eliminate $\mathrm{d}p$ and $\mathrm{d}h$ from the equations, we obtain

$$\frac{\mathrm{d}\rho}{\mathrm{d}B} = \frac{\{1-(\gamma_h-1)(E/uB-1)\}\,B}{\mu(u^2-a^2)}, \tag{15}$$

which may be compared with (11), the equivalent for a gas with $p/\rho = \text{const.}$ B is thus stationary at sonic points, but ρ is now stationary when $E/uB = \gamma_h/(\gamma_h-1)$ instead of when $B = 0$. The condition $E/uB = \gamma_h/(\gamma_h-1)$ was found to be of particular significance in the low-magnetic-Reynolds-number analysis of Resler & Sears (1958). Here the possibility of there being states where both $E/uB = \gamma_h/(\gamma_h-1)$ and $u = a$, so that $\mathrm{d}\rho/\mathrm{d}B$ cannot be determined directly from the above equation, will be found to be of major significance for all values of magnetic Reynolds number.

At a point on a (B,ρ)-curve where the tangent passes through the origin, so that $\mathrm{d}\rho/\mathrm{d}B = \rho/B$, the above equation gives

$$u^2 = a^2 + \{1-(\gamma_h-1)(E/uB-1)\}\,(B^2/\mu\rho), \tag{16}$$

which may be compared with (12) for a gas with $p/\rho = \text{const.}$ It follows that the flow velocity only equals the magnetoacoustic speed $(a^2+b^2)^{\frac{1}{2}}$ at the tangent point if we have the additional condition $E/uB = 1$ there.

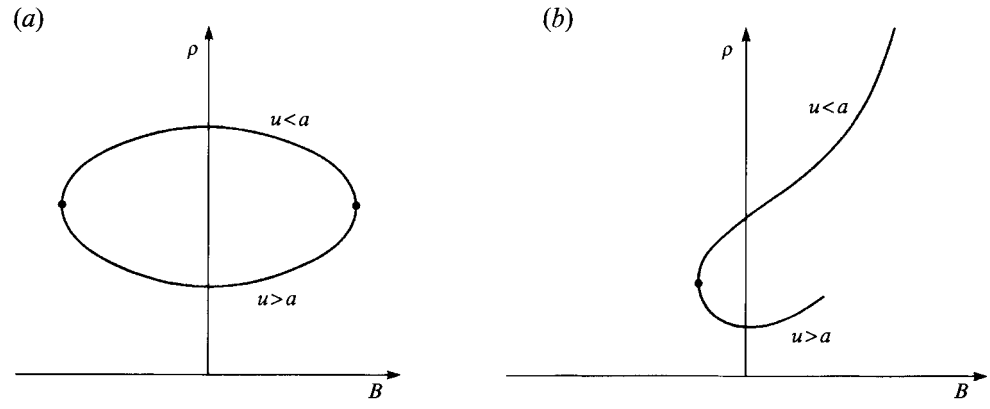

FIGURE 3. (B,ρ)-variation for special cases. (*a*) Fanno-type process (G and H const. while F varies, being a minimum at $u = a$). (*b*) Rayleigh-type process (G and F const. while H varies, being a maximum at $u = a$). ●, Sonic point.

Making now the assumption that the gas is perfect with constant ratio of specific heat capacities γ, the parameter γ_h, as defined above, may be identified with $\gamma(= a^2/\partial p/\partial\rho)_T$ and also with the isentropic index $(= a^2/(p/\rho))$. We then have for such a gas

$$h = \{\gamma/(\gamma-1)\}p/\rho, \quad a^2 = \gamma p/\rho, \tag{17}$$

and the energy equation (8) may be written as

$$\frac{\gamma-1}{\gamma}\rho H = p+\frac{\gamma-1}{2\gamma}\rho u^2 = \frac{\gamma-1}{\gamma}\rho(H^0 - EB/\mu G). \tag{18}$$

Eliminating p and u by means of continuity (7) and momentum (8), we obtain

$$\frac{\gamma+1}{2\gamma}\frac{G^2}{\rho}+\frac{\gamma-1}{\gamma}H^0\rho+\frac{1}{2\mu}\left(B-\frac{\gamma-1}{\gamma}\frac{E}{G}\rho\right)^2 = F^0+\frac{1}{2\mu}\left(\frac{\gamma-1}{\gamma}\frac{E}{G}\rho\right)^2 \tag{19}$$

and again a comparison may be made with the equivalent equation (10) for a gas with $p/\rho = \text{const}$. Note that, for given ρ, the equation is quadratic in B, the two values being symmetrically disposed about $\{(\gamma-1)/\gamma\}(E/G)\rho$. This also confirms the fact that ρ is normally stationary when $B = \{(\gamma-1)/\gamma\}(E/G)\rho$. Equation (19) yields a cubic in ρ for the values at the stationary points, the products of the roots being positive, so that there is the possibility of three such points occurring in a plot of ρ against B.

Closer inspection of (19) reveals that it is quadratic in ρ for given B also. This corresponds to the fact that F and H are directly determined from B by (9) and (8) and states that occur on either side of a shock wave are related by G, F and H being the same on each side. It then follows from the properties of shock waves that there cannot be more than two states for given B, one being subsonic (at the greater value of ρ) and the other supersonic.

Although the variation of ρ with B for a perfect gas is embodied in (19), the shapes of all possible solution curves in the (B,ρ)-plane are not immediately obvious, and a further consideration is the fact that the equation by itself carries no information about whether a particular value of ρ corresponds to a real gas state, e.g. it may turn out that the pressure is negative. In Appendix A of the appendices available on request, it is shown how the variation of gas properties with varying B for given G, F^0, H^0 and E may be obtained from a study of process curves in the (F,H)-plane in a similar manner

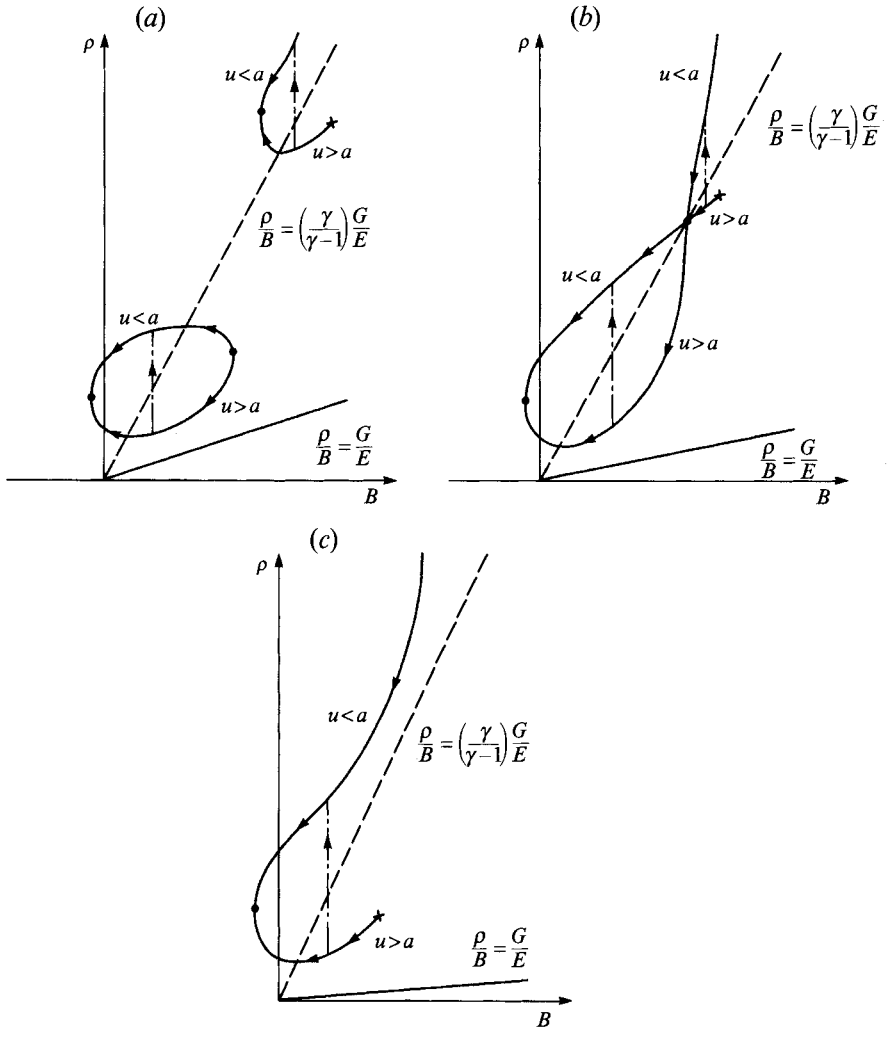

FIGURE 4. The three types of (B, ρ)-curve for the flow of a perfect gas in a duct of constant cross-sectional area. (*a*) A closed-loop lower branch with the possibility of an upper branch. (*b*) A transitional case with upper and lower branches merging at a cross-over point. (*c*) An open curve with $\rho \to \infty$ at one end and B a minimum at the only sonic point. ———, Possible shock-wave transition; ●, sonic point; +, point where $p = 0$.

to the investigation of other magnetogasdynamic processes (Cowley 1963, 1967). Without further justification here we present sketches in figure 4 of the three main types of (B, ρ)-curve that are found to occur. They are as follows.

(*a*) A closed loop with two sonic points and two points where ρ is stationary, qualitatively similar to the curve for a gas with $p/\rho = \text{const.}$ or to a Fanno process, but no longer symmetrically disposed about the ρ-axis. There is the possibility of a separate upper branch, on which there is a third sonic point, B being a minimum there. The supersonic part of the upper branch terminates at a point where pressure falls to zero and there may or may not be a point where ρ is stationary. An important feature to note because of its consequence for the subsequent analysis is that the upper-branch sonic point must occur where $uB/E = GB/\rho E < (\gamma - 1)/\gamma$, i.e. to the left of the dashed line on figure 4(*a*) while the lower-branch B-maximum point must occur where

$uB/E < (\gamma-1)/\gamma$. In general it is possible for some of the lower loop to be excluded because pressure becomes negative, but not in the context of the thruster problem.

(*b*) A transitional case, where the lower loop merges with the upper branch at what we shall refer to as a crossover point. Conditions at the crossover are such that both $u = a$ and $uB/E = (\gamma-1)/\gamma$, so that $\mathrm{d}\rho/\mathrm{d}B$ (equation (15)) may be finite and non-zero.

(*c*) An open curve with B reaching a minimum at a sonic point where $uB/E < (\gamma-1)/\gamma$ while ρ extends to infinity on the subsonic part of the curve and the supersonic part terminates at a point where $p = 0$. The curve is qualitatively like that of a Rayleigh process.

Ohm's law in the form quoted for $p/\rho = \text{const.}$ is still appropriate (equation (13)) and it follows that the variation of B and ρ with distance along the duct must be as shown by the arrows on figure 4, assuming the curves lie to the left of the line on which $\rho/B = G/E$. We see that the type (*b*) curve gives a possibility that was not available for a gas with $p/\rho = \text{const.}$, namely continuous variation from a subsonic state on the upper branch through sonic at the crossover point to supersonic.

Another interesting possibility arises from the fact that the (B, ρ)-curves are no longer symmetric about the ρ-axis, as they were for a gas with $p/\rho = \text{const.}$ Appropriate values of G, F^0 and H^0 allow the curve to touch the ρ-axis so that the end condition ($B = 0$) can be satisfied at a sonic point. We may therefore have subsonic flow in a duct leading to sonic exit.

4. Determining flow behaviour for thrusters

We now consider the general behaviour of our one-dimensional adiabatic flows as they might occur in thrusters and determine the parameter ranges for the different types of flow. As for §3 the discussion will be limited to the essential points and further details may be found in Appendix B of the appendices available on request from the Editorial Office.

The magnetic field at entry to the MHD duct B_0 is taken to be specified (i.e. the total current is given – see §1) and the state of the gas in the upstream plenum chamber is also taken to be specified (i.e. stagnation conditions at entry to the duct are given). As in the discussion for a gas with $p/\rho = \text{const.}$, it is assumed that between the plenum chamber and the start of the MHD duct the passage is converging, so that the entry flow cannot be supersonic, and that the pressure beyond the end of the duct is so low that exit flow cannot be subsonic. Flows with exit Mach number less than unity may certainly exist if the pressure is matched to the external value, but they are not considered here.

One other condition is needed to determine the flow in the MHD duct and that in practice might well be its length. However, in the context of a general analysis of (B, ρ)-variation, length is only found as a final step by integration of Ohm's law. For the purpose of determining parameter ranges in which different types of flow occur, we take the remaining condition to be a specified value of electric field. It is to be expected that increasing the electric field is in some sense equivalent to shortening the duct, i.e. as the impedance of the thruster is increased, more voltage will be needed to drive the current associated with the given magnetic field.

With B_0, E and plenum-chamber conditions being the significant physical properties, a possible approach to characterizing thruster behaviour might be to take the ratio of initial magnetic pressure to plenum pressure p_p as one non-dimensional parameter, $B_0^2/2\mu p_p$. We choose, in fact, to take what is equivalent, namely $B_0^2/\mu\rho^* u^{*2}$, where ρ^* and u^* are values of density and velocity that would be achieved by adiabatic reversible

(B,ρ)-curve		Entry	Exit	Flow pattern
a (lower loop)	(i)	sonic	supersonic	supersonic/magnetosonic/ supersonic
	(ii)	sonic	supersonic	supersonic
	(iii)	sonic	sonic	supersonic/shock-wave/ subsonic
	(iv)	subsonic	sonic	subsonic
b	(v)	crossover	supersonic	supersonic
	(vi)	subsonic (above crossover)	supersonic	subsonic/crossover/ supersonic/magnetosonic/ supersonic
	(vii)	subsonic (above crossover)	supersonic	subsonic/crossover/ supersonic
	(viii)	subsonic (above crossover)	sonic	subsonic/crossover/ supersonic/shock-wave/ subsonic
	(ix)	subsonic (below crossover)	sonic	subsonic
c	(x)	subsonic	sonic	subsonic

TABLE 1. Flow types in the MHD duct

expansion to sonic conditions from the plenum chamber (i.e. they are the inlet values to the duct if the entry is actually sonic). The relation of $\rho^* u^{*2}$ to plenum pressure is given by the usual results for one-dimensional isentropic flow with area variation as

$$\rho^* u^{*2} = \gamma \left\{ \frac{2}{(\gamma+1)} \right\}^{\gamma/\gamma-1} p_p. \tag{20}$$

We choose the electric-field parameter to be $E/u^* B_0$ and we shall take $\gamma = \frac{4}{3}$.† In the following analysis we shall use the notation

$$\beta^* = \frac{B_0^2}{\mu \rho^* u^{*2}}, \quad \lambda^* = \frac{E}{u^* B_0}, \tag{21a}$$

i.e. β^* and λ^* are taken as the non-dimensional groups which determine thruster behaviour. However, it will be convenient to refer on occasion to groupings based on local properties at a particular state, e.g. if the state is designated state 1,

$$\beta_1 = \frac{B_1^2}{\mu \rho_1 u_1^2}, \quad \lambda_1 = \frac{E}{u_1 B_1}. \tag{21b}$$

Reference to the (B,ρ)-curves of figure 4 shows that the entry and exit conditions may be satisfied by a variety of flows. These are listed in table 1 and paths on the (B,ρ)-plane are shown as insets on figure 5. Note that use is being made of the two possibilities mentioned at the end of §3, namely transition from subsonic flow in the duct to supersonic via a crossover point and sonic exit following subsonic flow.

Of the flows listed in table 1, *a*(i), *a*(iii), *b*(vi) and *b*(vii) are distinguished by having two states where specific relations hold, e.g. $u = a$ where $B = 0$ is the relation at a sonic exit state. The condition for a crossover point in the flow requires that $u = a$ where $E = uB$, but, if that point is at entry, there are effectively two relations since $B = B_0$ also.

† The value of γ has been chosen somewhat arbitrarily. Ionizing gases have a low effective γ, so that $\frac{5}{3}$, the value for a fully ionized gas would be too high.

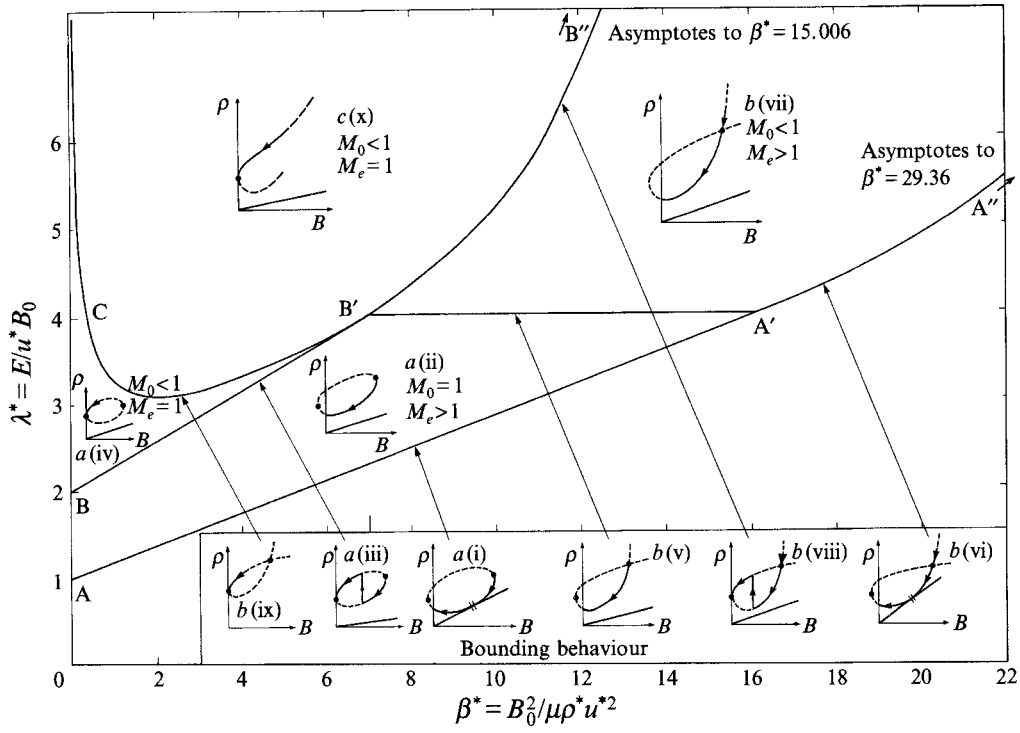

FIGURE 5. The parameter space $\beta^* = B_0^2/\mu\rho^* u^{*2}$, $\lambda^* = E/u^* B_0$, showing the (B,ρ)-variation that occurs in the various regions of that space when the duct is choked and the entry state has to have Mach number equal to or less than unity. The region below and to the right of line AA′A″ is inaccessible. On the line BB′B″ each point represents a range of possible processes with the same entry and exit states, but the position of a shock-wave transition is undetermined by the parameter values. On the inset (B,ρ)-curves (see also table 1): •, sonic point; \ \, magnetosonic point; ——, part of curve representing the process; – – – –, part of curve not involved in the process.

It follows that flow pattern b(v) may be placed in the same category as a(i), etc. The other flow patterns have only one specific state and it is to be expected that these occur for whole regions of the parameter plane (β^*, λ^*), while those with two specific states appear on lines separating those regions.

Denoting properties on two specific states by the subscripts 1 and 2, they are related by continuity (7), the integrated form of the momentum equation (9) and the integrated energy equation (8):

$$\rho_1 u_1 = \rho_2 u_2, \tag{22a}$$

$$p_1 + \rho_1 u_1^2 + B_1^2/2\mu = p_2 + \rho_2 u_2^2 + B_2^2/2\mu, \tag{22b}$$

$$h_1 + u_1^2/2 + EB_1/\mu\rho_1 u_1 = h_2 + u_2^2/2 + EB_2/\mu\rho_2 u_2. \tag{22c}$$

Introduction of the perfect-gas relations (17) and of the local parameters β_1 and λ_1, as defined by (21b) yields after rearrangement

$$\left(\frac{1}{\gamma M_1^2}+1\right)\frac{1}{\beta_1}+1 = \left(\frac{1}{\gamma M_2^2}+1\right)\frac{1}{\beta_1}\frac{u_2}{u_1}+\frac{B_2^2}{B_1^2}, \tag{23a}$$

$$\left(\frac{1}{(\gamma-1)M_1^2}+\frac{1}{2}\right)\frac{1}{\beta_1}+\lambda_1 = \left(\frac{1}{(\gamma-1)M_2^2}+\frac{1}{2}\right)\frac{1}{\beta_1}\frac{u_2^2}{u_1^2}+\lambda_1\frac{B_2}{B_1}, \tag{23b}$$

where M is the Mach number of the flow. If we now make particular specifications for

states 1 and 2, a relationship between β_1 and λ_1 (and consequently between β^* and λ^*) follows. Thus, for the flow pattern a(i) with sonic entry (state 1) and a magnetoacoustic point (state 2), the specific states require

$$M_1 = 1, \quad \beta_1 = \beta^*, \quad \lambda_1 = \lambda^*, \tag{24a}$$

$$1 = \frac{1}{M_2^2} + \beta_1 \frac{B_2^2 u_1}{B_1^2 u_2}, \quad \lambda_1 = \frac{u_2 B_2}{u_1 B_1}, \tag{24b}$$

where the relations of (24b) have been derived from $u_2^2 = a_2^2 + b_2^2/\mu\rho_2$ and $E = u_2 B_2$. Equations (23) linking the two states, together with the state specifications (24), provide seven equations for the eight variables M_1, M_2, B_2/B_1, u_2/u_1, λ_1, β_2, λ^*, β^*, and the expectation that there is a direct relation between β^* and λ^* for which type a(i) flow occurs has been fulfilled. The relation is plotted as the line AA′ on the parameter plane (β^*, λ^*) shown in figure 5. It terminates at A′ because at that point the (B, ρ)-curve switches to type b.

In a similar fashion other lines in the (β^*, λ)-plane corresponding to conditions for flows with two specific states may be found and they are reproduced on figure 5. Thus BB′ is the line for a type a(iii) flow and it is found from (23) with the relations

$$M_1 = 1, \quad \beta_1 = \beta^*, \quad \lambda_1 = \lambda^*, \tag{25a}$$

$$M_2 = 1, \quad B_2/B_1 = 0, \tag{25b}$$

1 being taken as the entry state and 2 as the exit. The system of equations for this case yields an explicit equation for the line, which is

$$\lambda^* = \frac{1}{8}\left(\frac{\gamma^2\beta^*}{\gamma^2-1} + \frac{4\gamma}{\gamma-1}\right). \tag{26}$$

Note that each point on BB′ represents a range of flows depending on the strength of the shock wave that is embedded in the flow. The apparent indeterminacy disappears when the situation is characterized by β^* and a magnetic Reynolds number based on duct length, since the length required for a given change in B, being controlled by the combination of Ampere's law and Ohm's law (13), depends on whether uB is low (subsonic) or high (supersonic). Thus the value of the magnetic Reynolds number depends on how much of the flow is subsonic as opposed to supersonic, i.e. on the position of the shock wave.

The line A′A″ on figure 5 represents type b(vi) flow with specific relations at a crossover point (state 1) and a magnetoacoustic point (state 2). These states require that

$$M_1 = 1, \quad \lambda_1 = E/u_1 B_1 = \gamma/(\gamma-1), \tag{27a}$$

$$1 = \frac{1}{M_2^2} + \beta_1 \frac{B_2^2 u_1}{B_1^2 u_2}, \quad \lambda_1 = \frac{u_2 B_2}{u_1 B_1}, \tag{27b}$$

and with (23) there are six equations for the six unknowns M_1, M_2, u_2/u_1, B_2/B_1, β_1 and λ_1. The values of the local parameters β_1 and λ_1 at the crossover are therefore fixed for all points on A′A″, being the same as β^* and λ^* at A′, where the crossover is at entry, i.e. at values 16.19 and 4 respectively (for $\gamma = \frac{4}{3}$). To find β^* and λ^* for points away from A′, it is necessary to work back from the crossover state to a compatible subsonic state using (23). In performing such calculations we found that the increase in β^* along A′A″ on figure 5 comes about not so much from the change in B between subsonic entry and the crossover point in the flow, which is comparatively small however low the entry Mach number, but rather from the influence of changing conditions on $\rho^* u^{*2}$. β^* tends to a maximum value of 29.36 as the entry Mach number is reduced to zero (and $\lambda^* \to \infty$).

The line B′B″, where the flow is of type b(viii) with a crossover (state 1) and sonic exit (state 2), has

$$M_1 = 1, \quad \lambda_1 = E/u_1 B_1 = \gamma/(\gamma-1), \tag{28a}$$

$$M_2 = 1, \quad B_2/B_1 = 0, \tag{28b}$$

and, like the situation on A′A″, the values β_1 and λ_1 are the same along the whole line, being 7 and 4 respectively ($\gamma = \frac{4}{3}$). Parameters β^* and λ^* are again found by working backwards from the crossover to compatible subsonic entry. β^* tends to 15.006 as the entry Mach number approaches zero and, at this limit, the ratio of B_0 (entry) to B at the crossover is 9/8, irrespective of the value of γ, while the ratio of magnetic pressure at entry to gas pressure $B_0^2/2\mu p_0$ is 27/5 and also independent of γ (see the discussion later, below (33)).

The types of flow indicated for the regions between the lines AA′A″ and BB′B″, and BB′B″ and the λ^*-axis, on figure 5 are then reasonable inferences, but Appendix B of the appendices which may be obtained from the Editorial Office of the *Journal* should be consulted for a fuller discussion of how flow types depend on values of β^* and λ^*.

An interesting feature of the map on the (β^*, λ^*)-plane is the fact that it extends indefinitely in the λ^*-direction. As mentioned above in connection with the lines A′A″ and B′B″, the Mach number at entry to the MHD duct tends to zero as $\lambda^* \to \infty$ on those lines. It is easily shown that, throughout the range of β^* at this limit and in relation to finite flow properties elsewhere in the duct, we may take entry values $u_0 = 0, a_0 = 0, \rho_0 \to \infty$, but $\rho_0 u_0$ ($= G$) and p_0 both non-zero and finite. The implication is that the only property of the gas state in the plenum chamber that has significance for the duct flow is the pressure p_p, which becomes equal to the entry pressure p_0 at this limit, since acceleration in the initial convergence is negligible. Energy supplied electrically to the gas in the duct is wholly dominant by comparison with the enthalpy in the plenum chamber. The parameter β^* can still be formed since $\rho^* u^{*2}$ depends only on the plenum-chamber pressure, but no other finite, non-zero, non-dimensional group that can be regarded as independent can be formed, nor is it possible to express velocity, density, etc., non-dimensionally using plenum-chamber properties only.

A scheme for making the variables non-dimensional which permits detailed analysis of the $\lambda^* \to \infty$ limit can be based on the assumption that G is specified rather than E. This was the scheme adopted by Kuriki *et al.* (1983). (For this reason and because the flow velocity is being raised from a negligible value compared to the exit velocity, we shall refer to this limit as the 'KKS limit'.) A characteristic velocity is defined by

$$u_k = B_0^2/2\mu G, \tag{29}$$

which would be the velocity achieved by the flow if pressure were zero initially and finally. A finite electric field parameter may then be formed as

$$\lambda' = E/u_k B_0. \tag{30}$$

It turns out that explicit equations can be found for λ' as a function of β^* in the KKS limit. To do this, we return to (22) relating properties at two states in the duct through continuity, momentum and energy, but in the basic form instead of the derived equations (23). Setting state 1 to be at entry to the duct ($u_1 = h_1 = 0, p_1 = p_0, B_1 = B_0$) and state 2 to be at a sonic point, we obtain

$$p_0 + \frac{B_0^2}{2\mu} = \frac{\gamma+1}{\gamma} G u_2 + \frac{B_2^2}{2\mu}, \tag{31a}$$

$$\frac{EB_1}{\mu G} = \frac{1}{2}\frac{\gamma+1}{\gamma-1} u_2^2 + \frac{EB_1}{\mu G}. \tag{31b}$$

For the range of β^* between B″ and A″, state 2 is taken as a crossover, so that $E = \gamma u_2 B_2/(\gamma-1)$, and, using this result to eliminate the electric field from (30) and (31*b*), we obtain after some algebra

$$\lambda' = \frac{4}{27}\frac{\gamma^2}{\gamma^2-1}\left\{1+\frac{18\mu p_0}{B_0^2}-\left(1-\frac{6\mu p_0}{B_0^2}\right)^{\frac{3}{2}}\right\} \quad \text{on} \quad \text{B″A″}. \tag{32}$$

For the range of β^* between the λ^*-axis and B″, state 2 is taken to be the exit state, so that $B_2 = 0$, and we obtain

$$\lambda' = \frac{1}{4}\frac{\gamma^2}{\gamma^2-1}\left(1+\frac{2\mu p_0}{B_0^2}\right)^2 \quad \text{left of B″}. \tag{33}$$

Note that at B″ both equations hold and eliminating λ' from (32) and (33) yields an equation for $2\mu p_0/B_0^2$ that does not contain γ. This confirms the assertion above that the ratio of magnetic pressure at entry to gas pressure at B″ is independent of γ and it is easily checked that the value of this ratio is 27/5.

To complete the algebra of the explicit expressions for λ' as a function of β^*, it is only necessary to relate p_0, which is the same as the plenum pressure p_p in the KKS limit, to $\rho^* u^{*2}$ using (20).

In §5.3 it will be seen how the magnetic Reynolds number of the duct based on u_k depends on λ' and β^*, so that the introduction of G to form a non-dimensional electric-field parameter is not as arbitrary as it seems at first. Since λ' is a function of β^* in the KKS limit, G becomes a function of β^*, B_0, the electrical conductivity σ and the length of duct L and is therefore determined by the values of these parameters.

5. Calculation of duct length and variation of properties with length

For the case of constant spacing between electrodes (G = const.) the length required to produce the boundary condition of zero flux at $x = L$ may be found by integration of the combination of Ampere's and Ohm's laws (13), i.e.

$$L = \int_0^L \mathrm{d}x = \int_{B_0}^0 \frac{\mathrm{d}B}{\mu\sigma(BG/\rho - E)}. \tag{34}$$

With ρ known as a function of B (essentially from the general (B,ρ)-equation (19)), the right-hand side can be evaluated numerically. The situation would be different if the electrode spacing were not constant and, with a view to possible future extensions of the theory, it is of interest to try a more direct approach to the basic equations (2)–(6). After rearrangement they lead to differential equations for the four properties B, u, ρ and p in terms of non-dimensional length, $\xi = x/L$, as follows:

$$\frac{\mathrm{d}B}{\mathrm{d}\xi} = r_m(uB-\lambda_0/s), \tag{35a}$$

$$\frac{\mathrm{d}u}{\mathrm{d}\xi} = \frac{1}{(\rho u^2-\gamma p)}\left\{\frac{pu}{s}\frac{\mathrm{d}s}{\mathrm{d}x}-\beta_0 r_m\left(\frac{\lambda_0}{s}-uB\right)\left((\gamma-1)\frac{\lambda_0}{s}-\gamma uB\right)\right\}, \tag{35b}$$

$$\frac{\mathrm{d}\rho}{\mathrm{d}\xi} = \frac{1}{(\rho u^2-\gamma p)}\left\{\frac{\rho}{s}\frac{\mathrm{d}s}{\mathrm{d}x}[(\gamma-1)p-\rho u^2]+\frac{\beta_0 r_m \rho}{u}\left(\frac{\lambda_0}{s}-uB\right)\left((\gamma-1)\frac{\lambda_0}{s}-\gamma uB\right)\right\}, \tag{35c}$$

$$\frac{\mathrm{d}p}{\mathrm{d}\xi} = -\frac{\rho u^2}{(\rho u^2-\gamma p)}\frac{\gamma p}{s}\frac{\mathrm{d}s}{\mathrm{d}x}+\beta_0 r_m\left(\frac{\lambda_0}{s}-uB\right)\left\{B+\frac{\rho u}{\rho u^2-\gamma p}\left((\gamma-1)\frac{\lambda_0}{s}-\gamma uB\right)\right\}. \tag{35d}$$

Here B, u, ρ and s have been non-dimensionalized by their entry values, and p by $\rho_0 u_0^2$ (subscript 0 again referring to entry to the MHD duct). The controlling non-dimensional parameters appearing in the equations are

$$r_m = \mu\sigma u_0 L, \quad \beta_0 = B_0^2/\mu\rho_0 u_0^2, \quad \lambda_0 = E_0/u_0 B_0, \tag{36a}$$

but in presenting results we shall be referring to starred quantities, as in (21a) of the last section, i.e.

$$r_m^* = \mu\sigma u^* L, \quad \beta^* = B_0^2/\mu\rho^* u^{*2}, \quad \lambda^* = E_0/u^* B_0, \tag{36b}$$

Numerical solutions of the equations have been obtained for $s = 1$. They rely nevertheless on the general understanding of possible flows developed in §4, i.e. for chosen values of β^* and λ^*, the regime on figure 5 (which type of (B,ρ)-curve) and the initial Mach number are determined. From these results β_0, λ_0 and the initial value of non-dimensional pressure p are evaluated. Solutions are then computed for various trial values of the magnetic Reynolds number r_m until one is found which gives B zero at exit, $\xi = 1$.

Two major sets of calculations were undertaken, for the parameter ranges

(i) $1.35 \leqslant \lambda^* \leqslant 3.2$ for $\beta^* = 1.75$, and

(ii) $2.67 \leqslant \lambda^* \leqslant 5.36$ for $\beta^* = 8.75$,

as detailed on figure 6, which shows again the (β^*, λ^*)-space of figure 5. The values were selected so as to illustrate the types of flow pattern listed in table 1.

5.1. *Calculations for* $\beta^* = 1.75$

For $\beta^* = 1.75$ the analysis of §4 shows that the range $1.35 \leqslant \lambda^* < 2.5$ relates to flows having entry Mach number M_0 unity and exit Mach number M_e supersonic with a type a (B,ρ)-curve. At the lowest value of λ^* (i.e. close to the line AA′ on figures 5 and 6) for which a successful computation was achieved, a high magnetic Reynolds number ($r_m^* = 173$) was required to give $B = 0$ at $\xi = 1$. Plots of non-dimensional B and ρ for this case are shown in figure 7(a) and illustrate the tendency towards formation of a magnetosonic plateau as $r_m^* \to \infty$. More representative plots of non-dimensional B and ρ are shown in figure 7(b) for $\lambda^* = 1.8$.

At $\lambda^* = 2.5$, $\beta^* = 1.75$, the operating condition is on the line BB′ of figures 5 and 6. The exit Mach number M_e is then unity according to the analysis of §4 and figure 7(c) shows the property variation for this case on both the completely supersonic route to exit and the completely subsonic route. Solutions were also computed for two values of λ^* greater than 2.5 (approximately 2.63 and 3.20 when $\mathrm{M}_0 = 0.8$ and 0.6 respectively). The distributions of B and ρ are not presented for the latter cases, but they are qualitatively like that of the subsonic-flow case at $\lambda^* = 2.5$. No difficulty was experienced in computing the direct solution of (35) by the step-by-step method when $\beta^* = 1.75$.

Plots of Mach-number variation along the duct length for various values of λ^* are shown together for comparative purposes on figure 8.

5.2. *Calculations for* $\beta^* = 8.75$

From the analysis of §4, it is found that for $\beta^* = 8.75$ flow in the duct will have sonic entry and supersonic exit and follow a type a (B,ρ)-curve if $2.6479 \leqslant \lambda^* < 4$. This was confirmed by the computed solutions for variation of properties with ξ, and, at the

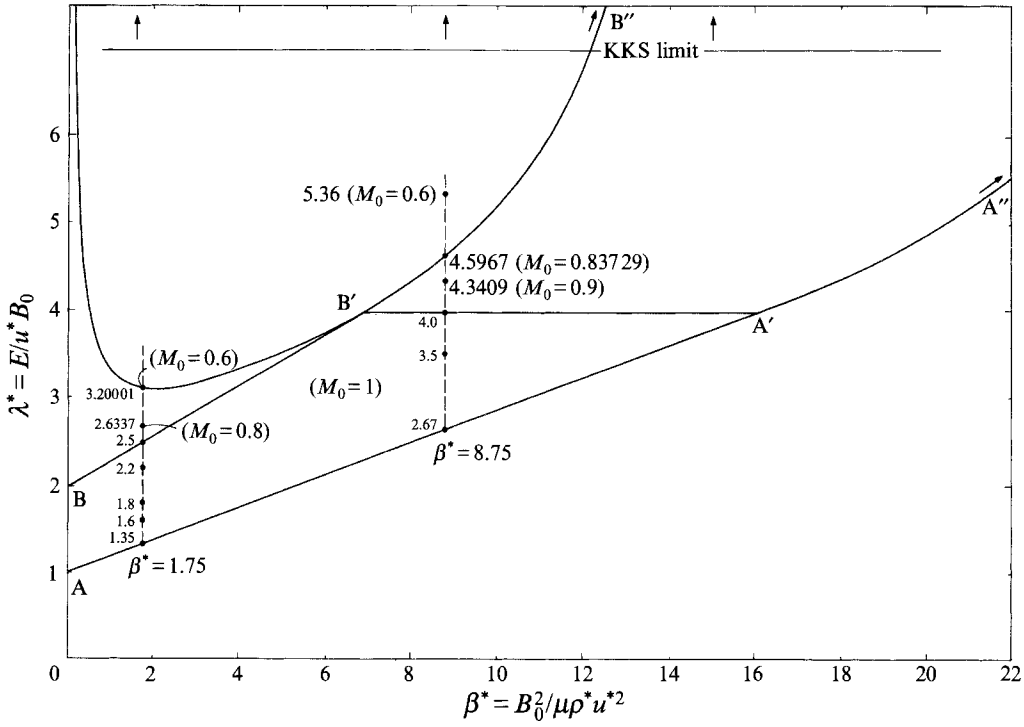

FIGURE 6. The (β^*, λ^*)-space, showing values of the parameters for which the equations have been integrated numerically. See figure 5 for the qualitative expectation of (B, ρ)-variation corresponding to each point.

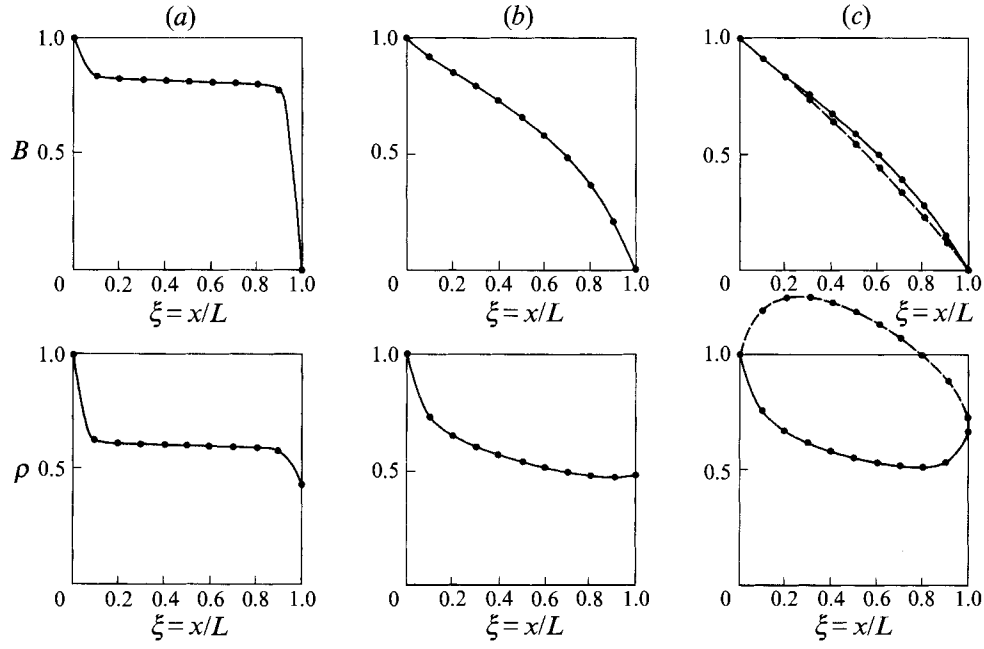

FIGURE 7. Variation of magnetic-field intensity and gas density with distance along the MHD duct for modest initial magnetic field ($\beta^* = B_0^2/\mu\rho^* u^{*2} = 1.75$). Increasing electric-field parameter λ^* ($= E/u^*B_0$) corresponds to reducing magnetic Reynolds number. (*a*) $\lambda^* = 1.35$; (*b*) $\lambda^* = 1.8$; (*c*) $\lambda^* = 2.5$; ——, supersonic; – – – –, subsonic.

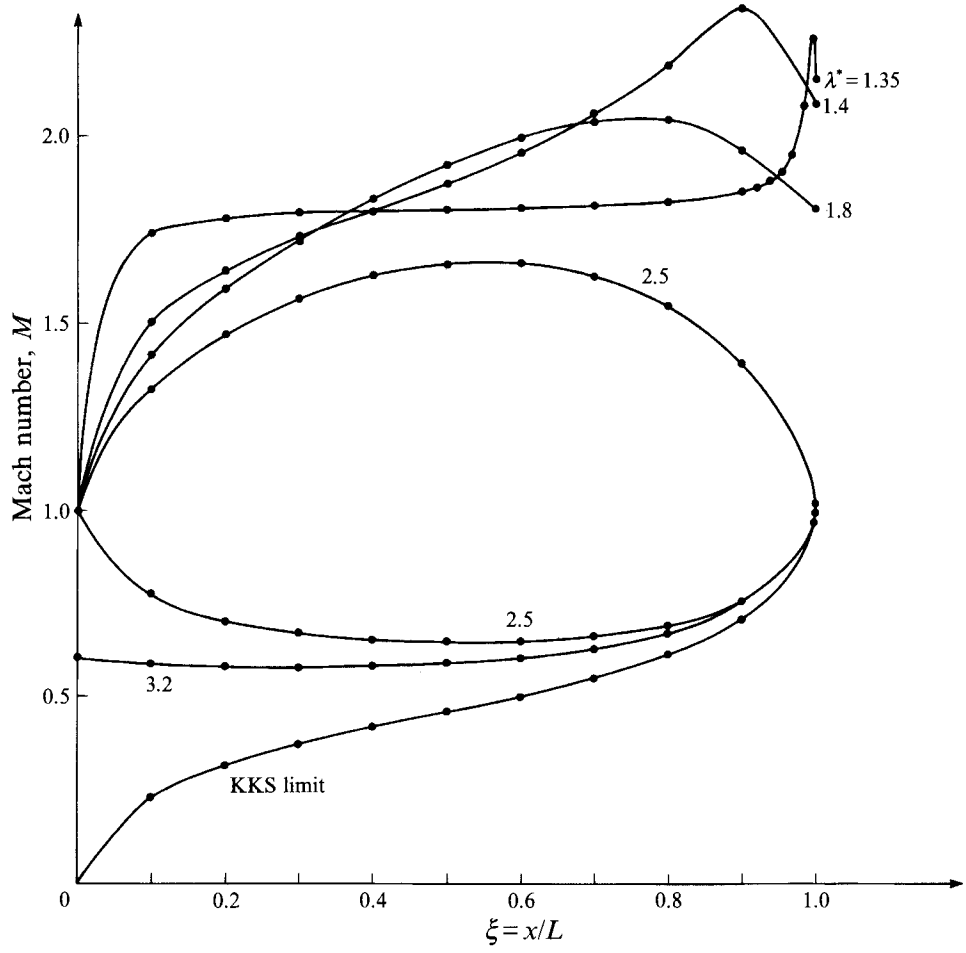

FIGURE 8. Mach-number variation along the MHD duct for $\beta^* = 1.75$ and various values of λ^*. With $\lambda^* = 2.5$ the possibility of shock-wave transition within the duct also exists, but no example of such a flow is shown.

lowest value of λ^* successfully attempted (2.67), the solution showed signs of the magnetosonic plateau being formed. The Mach-number distributions, for $\lambda^* = 2.67$, 3.5 and 4.0 are shown in figure 9(*a*).

Above $\lambda^* = 4.0$ up to $\lambda^* = 4.5967$, the analysis of §4 predicts that there will be subsonic entry, acceleration through a sonic state at a crossover point and then supersonic flow to the exit. It is perhaps not surprising that difficulty was experienced in getting the numerical solution to pass precisely through the crossover point and achieve supersonic flow. The tendency was for the computed solution to approximate to the subsonic part of the (B, ρ)-curve following that point. This is, of course, a valid solution of the equations, but one that does not fit the exit condition that we have assumed, namely that the flow must be supersonic or sonic at exit. The way in which the Mach number distributions with ξ were found was by running the computations from entry to a condition closely approximating to the crossover point and then re-starting the solution from a supersonic condition just after the crossover. The Mach-number distribution obtained in this way for $\lambda^* = 4.3409$ (entry Mach number $= 0.9$) is shown in figure 9(*a*) and it is of interest to see how small a region of the duct is associated with the subsonic pre-crossover flow.

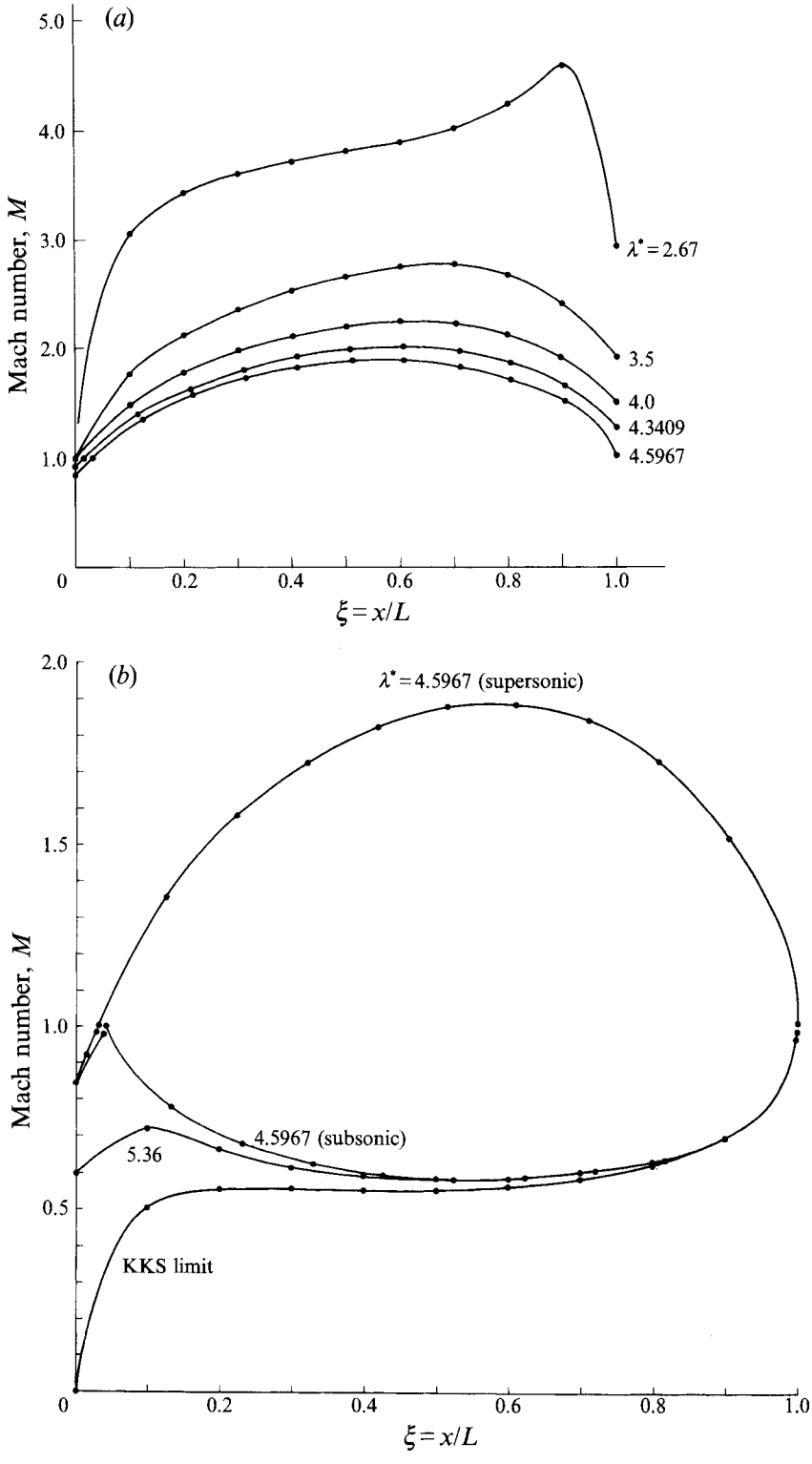

FIGURE 9. Mach-number variation along the MHD duct for a comparatively strong magnetic field ($\beta^* = 8.75$): (*a*) cases with some supersonic flow in the duct; (*b*) cases with no supersonic flow (except that for $\lambda^* = 4.5967$ the curve with some supersonic flow is included for comparison).

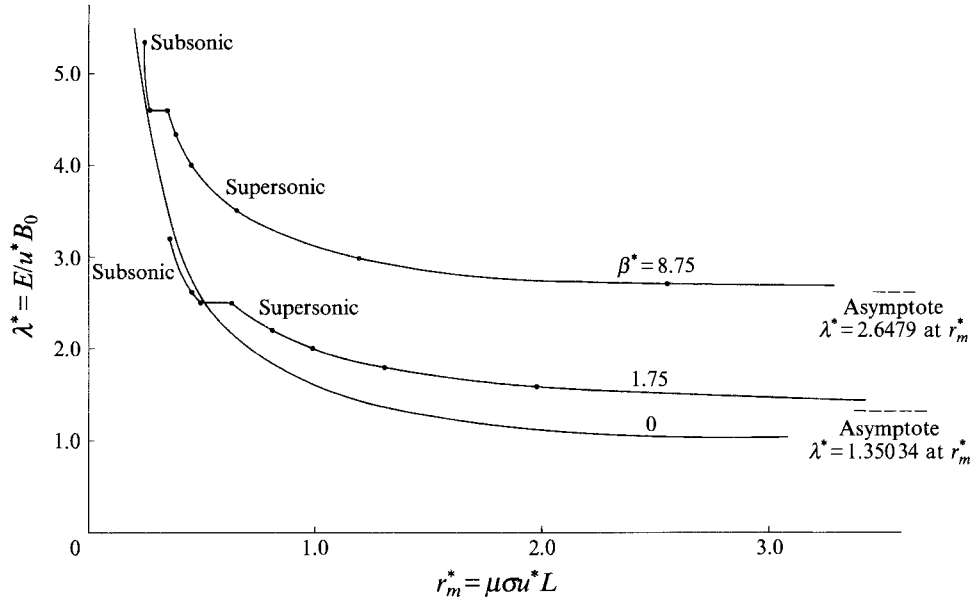

FIGURE 10. Value of electric-field parameter λ^* achieved as magnetic Reynolds number r_m^* of the duct is varied at $\beta^* = 0$, 1.75 and 8.75.

$\lambda^* = 4.5967$ at $\beta^* = 8.75$ corresponds to a point on the boundary line B′B″ in the (β^*, λ^*)-parameter-space of figures 5 and 6, so that for this λ^* there should after the crossover be a subsonic as well as a supersonic route to a sonic exit condition. The Mach-number distributions for both routes are compared on figure 9(*b*) in addition to that for the supersonic route being already shown on figure 9(*a*). Note that the vertical scales of figures 9(*a*) and 9(*b*) are different. Note also that the position ξ of the crossover point (where $M = 1$) is different for the two routes because the overall magnetic Reynolds number is different (magnetic Reynolds number based on distance from entry to crossover is the same). Included on figure 9(*b*) is the distribution for $\lambda^* = 5.36$, a case corresponding to a type *c* (B, ρ)-curve.

The relation between λ^* and magnetic Reynolds number r_m^* is plotted on figure 10 for $\beta^* = 1.75$ and 8.75. Note the steps in the curves where flow in the duct changes from supersonic to subsonic in the approach to sonic exit (boundary BB′B″ on figures 5 and 6); a shock wave would occur in the duct for values of r_m^* within the range of a step. For comparison we have included a curve that corresponds to $\beta^* \to 0$. At this limit, the electromagnetic effects have no influence on the flow, which for a constant-area duct following a convergence would maintain a constant velocity $u = 1$ in non-dimensional terms. By direct integration of (35*a*) for $\mathrm{d}B/\mathrm{d}\xi$ it follows that to satisfy the conditions $B = 1$ at $\xi = 0$ and $B = 0$ at $\xi = 1$

$$\lambda^* = \{1 - \exp(-r_m^*)\}^{-1},$$

and

$$B = \frac{1 - \exp\{r_m^*(\xi - 1)\}}{1 - \exp(-r_m^*)}. \tag{37}$$

The differences between this curve and those for $\beta^* = 1.75$, 8.75 are a measure of the influence of the 'back EMF' generated by the flow. The differences at low r_m^* (implying high λ^*) become small because the back EMF then has little influence and the

distribution of B approaches that expected in a stationary medium (i.e. linear – see figure 7(*c*) for an example showing this trend).

5.3. *Calculations of KKS-limit flows* ($\lambda^* \to \infty$)

As opposed to the analysis for a gas with $p/\rho = \text{const.}$, the perfect-gas analysis of §4 has shown that it is possible for the flow to enter an MHD duct with $M_0 < 1$, and at high λ^* may even approach what was referred to there as the KKS limit with $M_0 \to 0$. As suggested in §4, in order to make the equations non-dimensional at this limit we have adopted the approach of Kuriki *et al.* (1983) wherein mass flow per unit area G is used to define a characteristic velocity u_k ($= B_0^2/2\mu G$ – see (29)). Then velocity, density and pressure are made non-dimensional by u_k, G/u_k and Gu_k respectively, while the controlling parameters in the equations become

$$r'_m = \mu\sigma u_k L \quad \text{and} \quad \lambda' = E/u_k B_0. \tag{38}$$

The differential equations (35) are then recast to form

$$\frac{\mathrm{d}B'}{\mathrm{d}\xi} = r'_m(u'B' - \lambda'), \tag{39a}$$

$$\frac{\mathrm{d}u'}{\mathrm{d}\xi} = -\frac{2r'_m\{\lambda' - u'B'\}\{(\gamma-1)\lambda' - \gamma u'B'\}}{\rho' u'^2 - \gamma p'}, \tag{39b}$$

$$\frac{\mathrm{d}\rho'}{\mathrm{d}\xi} = \frac{2r'_m\rho'\{\lambda' - u'B'\}\{(\gamma-1)\lambda' - \gamma u'B'\}}{y'(\rho' u'^2 - \gamma p')}, \tag{39c}$$

$$\frac{\mathrm{d}p'}{\mathrm{d}\xi} = 2r'_m\{\lambda' - u'B'\}\left\{B' + \frac{[(\gamma-1)\lambda' - \gamma u'B']\rho' u'}{\rho' u'^2 - \gamma p'}\right\}, \tag{39d}$$

the assumption of constant electrode spacing having been taken. The entry conditions are now $u' = 0$, $\rho' = \infty$, but $\rho' u' = 1.0$. From the expression (29) for u_k, the starting value of p' is seen to be the ratio of plenum-chamber pressure to initial magnetic pressure. In turn the plenum-chamber pressure is directly related to $\rho^* u^{*2}$ by (20) (recall that $\rho^* u^{*2}$ is not zero for finite p_p although $\rho' u'^2$ at entry is), so that at entry p' is found from β^* by

$$p' = \frac{2}{\gamma\beta^*}\left(\frac{\gamma+1}{2}\right)^{\gamma/(\gamma-1)}. \tag{40}$$

By (32) and (33), λ' is determined as a function of β^*. Equations (39) are then solved in a similar manner to the previous computations, trial values of r'_m being taken and the equations integrated step by step until a value of r'_m is found that gives $B = 0$ at the end of the duct. Three values of β^* were selected for computation (1.75, 8.75 and 15.006). The first two values correspond to those used in the earlier calculations, and the third is the limiting value taken on the line BB′B″ in the (β^*, λ^*)-space of figures 5 and 6.

As expected, the first two calculations produced sonic flow at exit via a subsonic route (flow with a type *c* (B, ρ)-curve). The last calculation produced a sonic point near the duct entry, with subsequently either a subsonic route or a supersonic route to a sonic condition at exit (flow with a type *b* (B, ρ)-curve). Plots of the Mach-number distribution along the duct have been added to figures 8 and 9(*b*), for $\beta^* = 1.75$ and

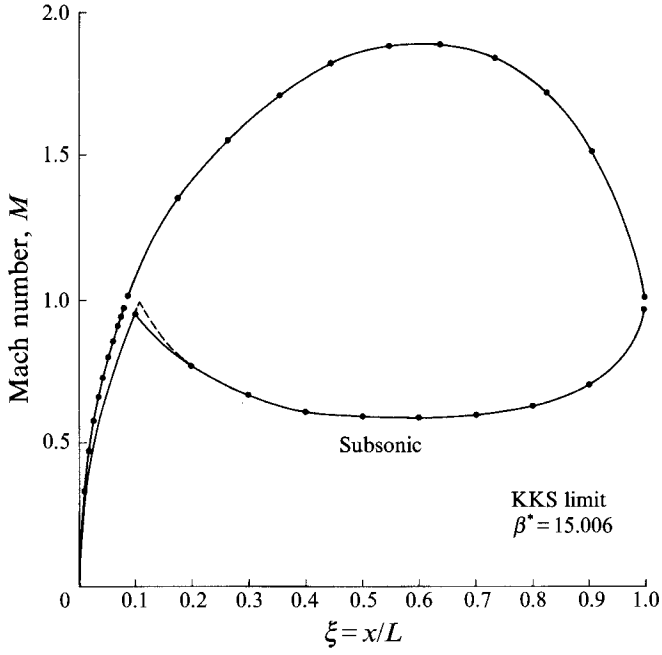

FIGURE 11. Mach number variation in the KKS limit for the case when β^* is just high enough (15.006) for supersonic flow in the duct to be a possibility. ——, Solutions obtained by integration of (39); – – –, check on subsonic solution by integration of (34).

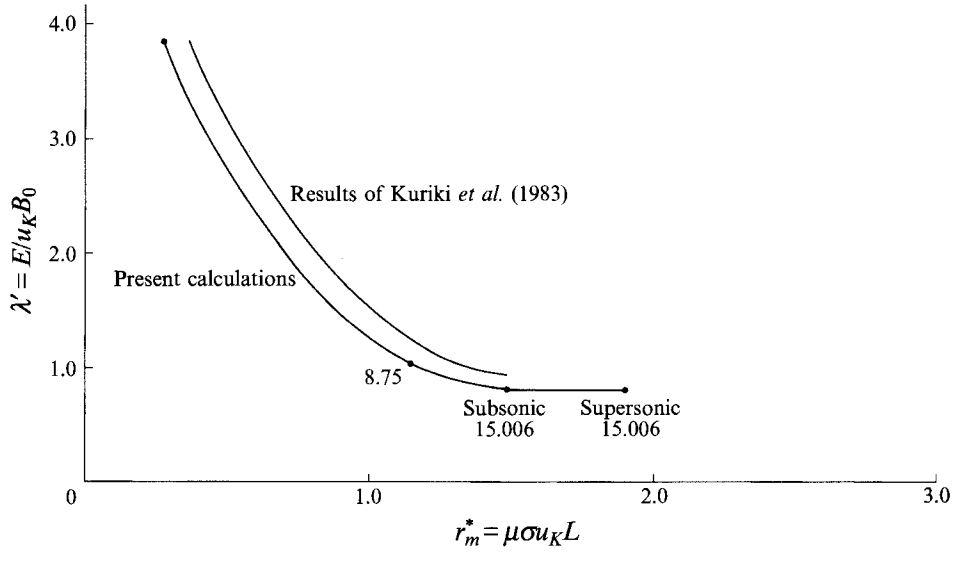

FIGURE 12. Value of electric-field parameter λ' against magnetic Reynolds number r'_m in the KKS limit.

8.75 respectively. Figure 11 shows the two Mach-number plots for the third value of β^* (15.006). As for the type *b* routes of figure 9(*b*), the position ξ of the crossover is different, depending on whether the flow is supersonic or subsonic after the crossover.

The final figure of this section (figure 12) shows the variation of λ' with r'_m for the KKS-limit calculations so that a direct comparison may be made with the results of

Kuriki *et al.* (1983).† It is clear that the difference between our line with the effect of pressure included in the analysis and that with pressure neglected is not great. However, we emphasize that in the KKS limit neither λ' nor r'_m are independent non-dimensional groups once β^* is specified. Figure 12, therefore, does not have the same kind of significance as figure 10, which may be interpreted as showing λ^* as a function of independent parameters r^*_m and β^*.

Although r'_m plays the role of a magnetic Reynolds number in (39*a*), its major significance in the present context is to act as a mass-flow parameter. Thus the definition of r'_m in (38) and the definition of u_k, (29), give

$$r'_m = \sigma B_0^2 L/2G. \tag{41}$$

If β^* is taken as the controlling non-dimensional group (i.e. specifying position along the upper boundary of figure 5), it may well be appropriate to take as the important dependent groups:

mass flow parameter $$G/\sigma B_0^2 L = 1/2r'_m, \tag{42a}$$

and voltage parameter $$\sigma\mu EL/B_0 = \lambda' r'_m, \tag{42b}$$

but these have not been plotted as functions of β^* since the information is implicit in figure 12 (note, however, that the voltage parameter is unity when back emf is negligible).

On the other hand it would certainly be reasonable to envisage a practical situation where G is the physically controlled quantity rather than the plenum-chamber pressure. This might be the case for a given feed to the plenum chamber, the pressure there being allowed to settle to whatever value is required for steady operation. Then r'_m and λ' are appropriate independent and dependent groups as they stand.

6. Concluding remarks on thruster performance

The analysis of flow in the MHD duct with the effect of gas pressure included has shown some features that correspond qualitatively with the findings of Kuriki *et al.* (1983), but there are striking differences. Of these the most immediate is the fact that there are no conditions under which it is valid to ignore pressure. As illustrated on figure 5 there is a limit to the value of the ratio of initial magnetic pressure to plenum-chamber pressure for which flows are possible (at $\beta^* = 29.36$ for $\gamma = \frac{4}{3}$, from which we may derive the ratio to be 10.57 using (20)). Since the ratio was found to be independent of γ at point B″ (see the end of §4), there is an indication that the limited range is a general feature whatever gas laws are assumed (although, to obtain the particular value 27/5 for the ratio at B″, assumptions that h and p/ρ are proportional to a^2 are still required).

At the downstream end of the duct the analysis has shown that above BB′B″ on figure 5 the exit state is sonic, so that pressure there remains comparable with the momentum flux per unit area. Even for the regimes between BB′B″ and AA′A″, for which the exit states are supersonic, the maximum exit Mach number achievable occurs at the limiting point A″, the value being 3.051 for $\gamma = \frac{4}{3}$ and the ratio of momentum flux per unit area to pressure is 12.41.

It is clear therefore that the pressure in the plenum chamber makes some contribution to the thrust produced by the MHD duct, whatever the operating condition. To reinforce some of the points that have emerged from the present analysis,

† Our λ' is twice their voltage parameter ϕ and our r'_m is one half their R_m. ϕ, R_m and their definitions were referred to in §1. See also (41) later for r'_m in terms of basic properties.

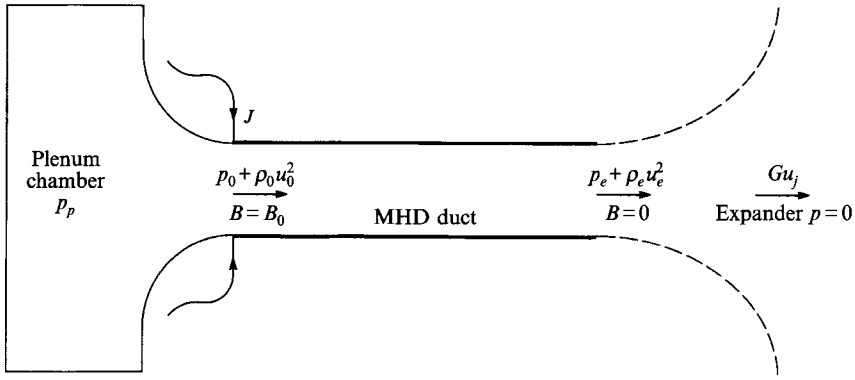

FIGURE 13. Arrangement of a thruster. The dashed lines indicate a diverging section, which might be added to increase thrust by allowing the gas to expand to negligible pressure after the MHD duct. The build-up of thrust per unit area of MHD duct is indicated by the $(p+\rho u^2)$ expressions and Gu_j.

we conclude with a brief discussion on thrust and the efficacy of the duct for this purpose. In this context there is a well-recognized modification to the geometry which will increase the thrust at any operating condition, namely to add a diverging section so that after exit from the MHD duct the gas will expand to the negligible pressure which we take to be ambient (e.g. see Shapiro 1953). This is illustrated schematically in figure 13 and we shall assume the area ratio across any such divergence approaches the ideal, i.e. it approaches infinity.

There are three essential components in the production of thrust per unit cross-sectional area of the MHD duct T/A. First is a component associated with the plenum-chamber pressure and the impulse that can be generated at the end of the inlet convergence:

$$\frac{T_1}{A} = p_0+\rho_0 u_0^2 = \frac{B_0^2}{2\mu}\frac{1}{\beta^*}C_1, \tag{43}$$

where

$$C_1 = 2\left\{\frac{1+\gamma M_0^2}{\gamma}\right\}\left\{\frac{\gamma+1}{2+(\gamma-1)M_0^2}\right\}^{\gamma/(\gamma-1)}. \tag{44}$$

This thrust is transmitted to the structure by the action of pressure on the walls of the plenum chamber and initial convergence. The second thrust component is given by the rise in impulse across the MHD duct

$$T_2/A = p_e+\rho_e u_e^2-p_0-\rho_0 u_0^2 = B_0^2/2\mu, \tag{45}$$

where subscript e refers to the state at duct exit. We then have $T_2/T_1 = \beta^*/C_1$. T_2 is transmitted to the structure by the mechanical supports of the wiring and electrodes. The third component is due to the final expansion in the added diverging section:

$$T_3/A = \rho_e u_e u_j - p_e - \rho_e u_e^2, \tag{46}$$

where u_j is the velocity of the final jet and may be found from the fact that the final kinetic energy $\frac{1}{2}u_j^2$ is the same as the stagnation enthalpy at duct exit $h_e+\frac{1}{2}u_e^2$. The effect of the divergence is best expressed in terms of a factor C_3, such that

$$T/A = T_1/A+T_2/A+T_3/A = (T_1/A+T_2/A)\,C_3, \tag{47}$$

where

$$C_3 = \frac{\gamma M_e\{2+(\gamma-1)M_e^2\}^{\frac{1}{2}}}{(\gamma-1)^{\frac{1}{2}}(1+\gamma M_e^2)}. \tag{48}$$

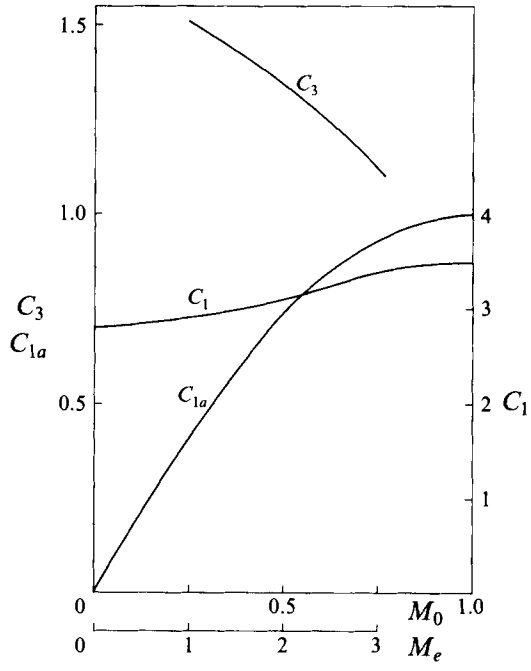

FIGURE 14. Dependence of C_1 and C_3 of (49) on entry Mach number M_0 and exit Mach number M_e respectively. Also dependence of C_{1a} of (51) on entry Mach number.

This final thrust component is transmitted to the structure by the action of pressure on the walls of the divergence. From (43), (45) and (48) we obtain

$$\frac{T}{A} = \frac{B_0^2}{2\mu}\left(\frac{C_1}{\beta^*} + 1\right) C_3. \tag{49}$$

C_1 and C_3 are plotted as functions of M_0 and M_e respectively for $\gamma = \frac{4}{3}$ on figure 14. If no divergence is fitted, (49) with C_3 set equal to unity gives the total thrust per unit cross-sectional area.

It will be seen from (49) and figure 14 that for values of β^* somewhat greater than unity the first thrust component makes only a modest contribution, the overall thrust per unit area without a divergence being not very different from that predicted by Kuriki *et al.* (1983), namely $B_0^2/2\mu$. However, the factor associated with the divergence can be significant since we have found that over much of the range of possible operating conditions the exit Mach number is unity. C_3 is then equal to 1.512. Even at the highest possible value of M_e (quoted above as 3.051 at A″), C_3 equals 1.187 and the diverging section provides nearly 20% amplification of thrust.

The major advantage of using MHD techniques in a thruster comes about not so much from the increase in thrust (that can be achieved by increasing plenum pressure or size), but rather from an increase in specific thrust (thrust per unit mass flow rate). When the flow regime is such that the Mach number at entry is unity (region ABB′A′ on figure 5), the mass flow rate is fixed by the plenum-chamber conditions and the cross-sectional area of the duct, while thrust is increased by the electromagnetic forces above the no-field condition, but only to a limited extent. A substantial improvement only occurs when the electromagnetic effects compel the entry Mach number to be significantly less than unity, i.e. for conditions approaching the KKS limit.

Specific thrust T/m may be found from the expression for T/A in (49) divided by ρu, but a more direct and enlightening approach is to work directly from overall energy considerations (the two methods give the same result because of the link provided by conservation equations having been satisfied within the MHD duct). For the case of a thruster fitted with a divergence T/m is just the velocity of the final jet u_j. We found u_j above by equating the kinetic energy of the jet to the stagnation enthalpy at duct exit, but it is also equal to the enthalpy in the plenum chamber plus the energy per unit mass added electromagnetically:†

$$u_j = \{2(h_p + EB_0/\mu G)\}^{\frac{1}{2}}.$$

To allow for a divergence not being fitted, we now need to divide by the factor C_3 of (53), so that

$$T/m = \{2(h_p + EB_0/\mu G)\}^{\frac{1}{2}}/C_3. \tag{50}$$

C_3 should therefore be given the value unity if there is a divergence, otherwise values are as in figure 14. Three components may again be recognized in the above equation: the effects of the plenum-chamber state, the MHD duct itself and the divergence, although they are not proportioned in the same way as for thrust per unit area. From the definitions (21 *a*) of λ^* and β^* and with the standard gasdynamic result for $G/\rho^* u^*$ in terms of Mach number, (50) may be rewritten as

$$\frac{T}{m} = \left(\frac{2EB_0}{\mu G}\right)^{\frac{1}{2}} \left(\frac{C_{1a}}{\lambda^* \beta^*} + 1\right)^{\frac{1}{2}} / C_3, \tag{51}$$

and values of C_{1a} ($= G/\rho^* u^*$) are given in figure 14 as a function of entry Mach number M_0 for $\gamma = \frac{4}{3}$.

High specific thrust is favoured by operation as close to the KKS limit ($r_m^* \to 0$) as is practical since this will give high E and low G. As has been seen in §4 the enthalpy of the gas in the plenum chamber can be neglected at that limit and $M_0 \to 0$ (or equivalently in (51) $\lambda^* \to \infty$ and $C_{1a} = 0$), so that specific thrust is related only to the energy added electro-magnetically per unit mass flow rate and to the effect of the divergence. It is interesting to find then that the value of β^* (i.e. the particular operating point) is immaterial in the KKS limit when high specific thrust is desired provided that a divergence is fitted. It can be achieved equally well at low values of β^* (i.e. near the λ^*-axis on figure 5, when acceleration by the electromagnetic forces has a weaker influence than the electrical heating) as at the higher permissable values. Low β^* implies that the thrust per unit area is associated mainly with T_1/A in (47) (see also (49)). It is then as if the MHD duct acts as a 'valve' limiting the flow rate while maintaining the thrust due to plenum-chamber pressure. However, if no divergence is fitted, there will be an advantage in operating the duct towards the higher end of the β^* range where the exit state is supersonic and the penalty of the C_3 factor is less than for sonic exit.

We should like to record our debt of gratitude to the late Arthur Shercliff, who introduced both of us to the fascination of MHD. It is many years since he kindled in us a particular interest in magnetogasdynamics, but it is a measure of the enthusiasm which he generated that the interest has endured.

† Kuriki *et al.* (1983) defined an efficiency as the ratio of kinetic energy in the jet to the electrical energy supplied, and its value is measure of the extent to which the supply power is divided between work done in accelerating the gas and ohmic dissipation. Here, all the electrical energy contributes to the rise in stagnation enthalpy and is in principle recoverable as kinetic energy.

REFERENCES

COWLEY, M. D. 1963 *J. Fluid Mech.* **15**, 577.
COWLEY, M. D. 1967 *J. Plasma Phys.* **1**, 37.
KURIKI, K., KUNII, Y. & SHIMIZU, Y. 1983 *AIAA J.* **21**, 322.
RESLER, E. R. & SEARS, W. R. 1958 *J. Aero. Sci.* **25**, 235.
SHAPIRO, A. H. 1953 *Compressible Fluid Flow*, Vol. I. Ronald Press.
SHERCLIFF, J. A. 1958 *J. Fluid Mech.* **3**, 645.
SHERCLIFF, J. A. 1965 *A Textbook of Magnetohydrodynamics*. Pergamon Press.